POTENTIAL CLINICAL RELEVANCE

Nanomedicine: Nanotechnology, Biology, and Medicine
8 (2012) 941–950

Research Article

nanomedjournal.com

Multifunctional nanoplatforms for fluorescence imaging and photodynamic therapy developed by post-loading photosensitizer and fluorophore to polyacrylamide nanoparticles

Anurag Gupta, BS[a], Shouyan Wang, PhD[b], Paula Pera, MSc[a], K.V.R. Rao, PhD[a], Nayan Patel, BA[a], Tymish Y. Ohulchanskyy, PhD[c], Joseph Missert, MSc[a], Janet Morgan, PhD[d], Yong-Eun Koo-Lee, PhD[b], Raoul Kopelman, PhD[b], Ravindra K. Pandey, PhD[a,*]

[a]*PDT Center, Buffalo, New York, USA*
[b]*Department of Chemistry, University of Michigan, Ann Arbor, Michigan, USA*
[c]*Institute of Lasers, Photonics and Biophotonics, University of Buffalo, New York, USA*
[d]*Department of Dermatology, Roswell Park Cancer Institute, Buffalo, New York, USA*

Received 13 July 2011; accepted 13 November 2011

Abstract

We report a novel post-loading approach for constructing a multifunctional biodegradable polyacrylamide (PAA) nanoplatform for tumor-imaging (fluorescence) and photodynamic therapy (PDT). This approach provides an opportunity to post-load the imaging and therapeutic agents at desired concentrations. Among the PAA nanoparticles, a formulation containing the photosensitizer, HPPH [3-(1′-hexyloxyethyl)pyropheophorbide-a], and the cyanine dye in a ratio of 2:1 minimized the undesirable quenching of the HPPH electronic excitation energy because of energy migration within the nanoparticles and/or Förster (fluorescence) resonance energy transfer (FRET) between HPPH and cyanine dye. An excellent tumor-imaging (NIR fluorescence) and phototherapeutic efficacy of the nanoconstruct formulation is demonstrated. Under similar treatment parameters the HPPH in 1% Tween 80/5% aqueous dextrose formulation was less effective than the nanoconstruct containing HPPH and cyanine dye in a ratio of 2 to 1. This is the first example showing the use of the post-loading approach in developing a nanoconstructs for tumor-imaging and therapy.

From the Clinical Editor: Fluorescence imaging is a rapidly evolving and relatively high-throughput tool currently only utilized in preclinical imaging. The authors of this work demonstrate a tumor-specific florescence imaging nanoplatform that enables not only imaging, but photodynamic therapy as well.

Key words: Near-infrared fluorescence imaging; Photodynamic therapy; Post-loading; Polyacrylamide nanoparticles

Both cancer detection and treatment depend on selective delivery of appropriate agents to the malignancy. Photodynamic therapy (PDT), a relatively new modality for the treatment of a variety of oncological, cardiovascular, dermatological, and ophthalmic diseases, is based on the preferential localization of photosensitizing molecules, (photosensitizers, PS) in target tissues.[1-5] On light activation, the PS produces reactive singlet oxygen,[5] which damages tumor cells and neovasculature, and also initiates antitumor inflammatory and immune responses.[6,7] We and others have developed relatively tumor-avid PS, which selectively accumulate in tumor, and these molecules have been used to carry optical, positron emission tomography (PET), and magnetic resonance (MR) imaging agents to the tumor sites.[8,9] However, the tumor selectivity of current PS is not always adequate. Approaches that link PS to antibody fragments or receptor ligands have been disappointing because the number of required PS/cell generally is greater than the number of antigen or receptor binding sites.[10] Conversely, the imaging agent carrying capacity of the individual PS molecules is limited.

Nanotechnology platforms potentially can deliver large numbers of PS and/or imaging agents.[11-13] Nanoparticles (NPs)

The authors declare no conflicts of interest. A part of the technology presented in this manuscript is licensed to Photolitec, LLC, Buffalo, New York.

Support was received from National Institute of Health grant CA119358 and the shared resources of the Roswell Park Cancer Center support grant CA16056.

*Corresponding author: Roswell Park Cancer Institute, PDT Center, Elm and Carlton Streets, Buffalo, NY 14263.

E-mail address: ravindra.pandey@roswellpark.org (R.K. Pandey).

1549-9634/$ – see front matter © 2012 Elsevier Inc. All rights reserved.
doi:10.1016/j.nano.2011.11.011

are uniquely promising in that (1) their hydrophilicity and charge can be altered; (2) they possess enormous surface area that can be modified with functional groups possessing a diverse array of chemical and biochemical properties, including tumor-selective ligands; (3) owing to their sub-cellular and sub-micron size, they can penetrate deep into tissues and are generally taken up efficiently by cells; (4) because numerous universal strategies for the preparation of nanomaterials are already in place, PS-loaded NPs can be made by numerous methods, such as covalent linkages and self-assembly.

We have recently shown that HPPH, developed in our laboratory[14-19] and currently under Phase I/II clinical trials, when conjugated with certain cyanine dyes can be used for both fluorescence imaging and photodynamic therapy.[20,21] The conjugate showed potential tumor imaging and PDT efficacy, but compared with the imaging dose the required therapeutic dose was eight-fold higher. Increasing the number of HPPH moieties in synthetic photosensitizer-cyanine dye (PS-CD) conjugates did not minimize the therapeutic dose.[20] We envision the comprehensive development, characterization and validation of multifunctional nanovector platforms that can deliver tumor-avid therapeutic photosensitizers that only become active (and toxic) when illuminated by specific wavelengths of light, and, in addition, carry one or more imaging agents; these nano-platforms thus could enable both diagnosis and image-guided therapy.

Among the NPs, hydrogel polyacrylamide (PAA) in which the monomeric units are linked together with ester bonds have been of particular interest because of their biocompatibility/biodegradability and low toxicity.[22,23] Using biodegradable polymer-based NPs avoids multi-step synthesis and has numerous advantages including the ability to create water soluble formulations with desired pharmacokinetic properties, capable of delivering a high payload of the multiple agents (therapeutic PS and imaging agents) to tumors, increased photostability of photoactive agents and fluorophores, and the ability to modify the surface of the NP for conjugation to a variety of biomolecules. NPs and other macromolecular objects can passively target the tumor interstitium, via the "enhanced permeability and retention" (EPR) effect because of the leaky vascular system in tumors.[24,25] In addition, the poor lymphatic drainage system in tumors causes fluid retention in the tumor interstitial space, which helps to retain polymeric NPs and other macromolecular objects in the tumor compared with normal tissue.[24,25] For these reasons, NPs are a promising means for delivering therapeutic and other molecular agents to tumors.

Because NPs could deliver a high payload of the drug to tumor, we investigated the use of a PAA-based nanoconstructs for delivering both the near-infrared (NIR) CD fluorophore and the red-light absorbing photosensitizer HPPH. The release of the desired imaging and therapeutic agents may also be controlled by creating an NP that is pH or temperature sensitive, or by modifying the pores of the NP matrix.[26] In a parallel study[27] we encapsulated the PS within polymeric NPs, but the retention efficiency was low, therefore a large concentration of NPs was required to achieve the desired therapeutic dose. To increase the retention of the PS within the NP, we decided to form the NPs first and then load the PS into the porous PAA-NPs. This novel loading approach of the desired agents was termed "*post-loading.*" In this procedure, both HPPH (phototherapeutic agent) and the CD (NIR fluorescence imaging agent) moieties were highly retained in the NPs (confirmed by release kinetics) and provided constructs for non-invasive detection of tumors and delineation of the tumor margins by NIR fluorescence imaging.

Fluorescence imaging is a non-invasive and non-ionizing imaging technique that requires only nanomoles of fluorophores for contrast enhancement.[24,25] The NIR spectral range (~650–950 nM) is known as the "biological window" for optical imaging because light absorption caused by water, deoxygenated hemoglobin, and oxygenated hemoglobin is minimized in this region, as well as tissue autofluorescence and light scattering.[12,13]

In this study we compared the photosensitizing and NIR fluorescence imaging potential of several biodegradable PAA NP formulations, in which the HPPH and CD moieties were post-loaded at a 2:1 and a 4:1 ratio, respectively. These formulations were significantly different in tumor uptake, in pharmacokinetics and in in vivo imaging and PDT efficacy.

Methods

Materials

Human serum albumin, Tween-80, and dimethyl sulfoxide (DMSO) were purchased from Sigma-Aldrich (St. Louis, Missouri). Bovine calf serum (BCS) was purchased and dPBS (pH 7.4, 1×, without calcium and magnesium) were purchased from Cellgro (Mediatech, Manassas, Virginia). Ethanol (200 proof) was purchased from Pharmco-Aaper (Shelbyville, Kentucky). All solutions were prepared with 18 MΩ water purified by a Millipore Milli-Q Advantage A10 water purification system. The 30-and 100-kDa Amicon Ultra-15 and Ultra-4 centrifuge filters were purchased from Fisher Scientific (Pittsburgh, Pennsylvania).

Animal studies

All animal studies were performed following the animal protocol guidelines approved by Institutional Animal Care and Use Committee (IACUC).

Synthesis of blank NPs

The PAA NPs were prepared by following our previous report with slight modifications (see Supplementary Materials, available online at http://www.nanomedjournal.com, for the synthesis).[26]

Post-loading of the PS 1, and the CDs 2, and 3 to blank AFPAA to create nanoconstructs 4, 5, 6, 9, and 10

In brief, 10 mg lyophilized PAA NPs were suspended in 1 mL of 1% Tween-80/water solution and to this solution 10 μL of 1, 2, or 3 (20 mM in DMSO) is added and magnetically stirred at a constant rpm for 2 hours. The NPs were centrifuge filtered in a 30-kDa Amicon Ultra-15 centrifuge filter for 30 minutes at 5000 RPM and then the NPs were reconstituted with water. The NPs were syringe filtered with a 0.2-μM regenerated cellulose syringe filter. Nanoformulation **9** and **10** were created by mixing nanoconstruct **1** and **3** such that the molar ratio of **1** to **3** was 2:1 and 4:1, respectively. The NPs are stored at 4°C until further use. For details see Supplementary Materials.

Post-loading of the PS 1 and the CD 3 to blank AFPAA to create nanoconstructs 7 and 8

On measuring the concentration of PS **1** in nanoconstruct **6**, CD **3** in DMSO (20 mM) was added such that the molar ratio of PS **1** to CD **3** was either 2:1 or 4:1. Once CD 3 was added, the procedure is the same as for post-loading, PS **1**, or CD **2** and **3**. For detailed procedure see the Supplementary Materials.

Release kinetics procedure

The in vitro release profile of the PS **1**, and the CD **3** in nanoconstructs/formulations **5**−**10** was measured. The NPs from all formulations were suspended in a 1% human serum albumin (HSA)—water solution and immediately the absorbance value for the HSA/nanoconstruct solution were measured spectrophotometrically. To measure the release of the PS **1** and/or the CD **3** from the NP, the NP solution is centrifuge filtered in a 100-kDa Amicon Ultra-4 centrifugation filter for 20 minutes at 4000 RPM. The absorbance of the PS or fluorophore in the filtrate was spectrophotometically measured (filtrate 1). The NPs in the retentate were reconstituted to the original volume with 1% HSA and re-centrifuge filtered (filtrate 2) and measured spectrophotometrically. The amount of **1** and/or **3** retained by the NP was confirmed by measuring the absorbance of the retentate on reconstitution to the original volume with 1% HSA. If the sum total of all filtrates and the retentate is less than 90% of the stock value for either chromophore, then ethanol is added to the centrifuge filter to measure what had adsorbed to the filter. These measurements were taken immediately post-addition of the nanoconstructs in a 1% HSA solution, **4** and 24 hours post-addition of the nanoconstructs in the 1% HSA solution. In addition the release of PS 1 and CD **3** in nanoconstruct **7** was measured in 25% BCS at 37°C. The procedure followed for the release of the PS/fluorophore in 25% BCS was similar to that of 1% HSA, except that the measurements were taken at 4, 8, 12, and 24 hours post-addition of nanoconstruct 7.

Optical imaging setup

The fluorescence imaging was conducted in accordance with a protocol approved by the IACUC at Roswell Park Cancer Institute and the Guide for the Use of Laboratory Animals. BALB/c mice (three mice/group) bearing subcutaneous Colon 26 tumors on the right shoulder were injected intravenously (tail-vein) with either CDs or nanoconstructs/-formulations. For a detailed description of the groups of mice imaged along with the dose, see the Supplementary Materials.

Absorbance, fluorescence, and singlet oxygen measurements

The absorbance measurements were performed on a Varian Cary-50 Bio Ultraviolet (UV)-Visible spectrophotometer. The concentrations of the NP formulations were measured in ethanol using 47,500, 200,000, and 207,455 L mol^{-1} cm^{-1} as the respective molar extinction coefficients of **1**, **2**, and **3**.

A SPEX 270M spectrometer (Jobin Yvon, Longjumean, France) was used for acquisition of fluorescence emission spectra in the far red and NIR spectral ranges, using the first output port equipped with an InGaAs photodetector (Electro-optical Systems Inc., Phoenixville, Pennsylvania). A diode-pumped solid-state laser (Verdi, Coherent Inc., Santa Clara, California) at 532 nM was the excitation source. Generation of singlet oxygen ($^1O_2$) was detected by its phosphorescence emission peaked at 1270 nM. The decays of this emission were acquired using the Infinium oscilloscope (Hewlett-Packard, Palo Alto, California) coupled to the output of the Hamamatsu IR-PMT, which is attached to the second output port of the SPEX 270M spectrometer. Nanoconstructs **5**−**8** in polystyrene cuvettes were placed in front of the entrance to the spectrometer. The emission signal was collected at 90-degrees relative to the exciting laser beam with the use of additional long-pass filters (a 950LP filter and/or a 538AELP filter) to attenuate the scattered light and fluorescence from the samples. A second harmonic (532 nM) from the nanosecond pulsed Nd:YAG laser (Lotis TII, Camarillo, California) operating at 20 Hz was used as the excitation source for time-resolved measurements.

In vivo photodynamic therapy

Eight-to 12-week-old BALB/cAnNCr mice (Jackson Laboratory, Bar Harbor, Maine) were inoculated subcutaneously with 1×10^6 Colon 26 cells. When tumors reached 40−70 mm^3, mice were injected intravenously (tail vein) with PS **1** (formulated in 1% Tween 80/D5W) or PAA nanoconstructs/formulations **6**−**10** suspended in water and further diluted in D5W. After 24 hours after intravenous injection (dose of PS **1**: 0.47 μmol/kg), mice (BALB/c mice bearing Colon 26 tumors, ten mice/group) were restrained in plexiglass holders and tumors were irradiated at 665 nM with a fluence and fluence rate of 135 J/cm^2 at 75 mW/cm^2, respectively, using a pumped argon-dye laser. The growth of tumors was measured two to three times per week and the mice were monitored for a total of 60 days post-PDT treatment. When the tumor regrowth was >400 mm^3, the mice were euthanized according to the guidelines of the institute-approved animal protocol.

Results

Preparation of HPPH and NIR CD post-loaded PAA NPs

In an ongoing SAR study with a series of CDs, we modified IR820 **2** with limited imaging potential to a highly avid CD **3** in which the chloro-group of IR820 was replaced with a *p*-aminothiol functionality. CD **3** formulated in 1% Tween 80/5% dextrose was tumor avid, but the corresponding PAA formulation produced enhanced tumor contrast. On the other hand PS **1** (HPPH) and nanoconstruct **6** showed similar PDT efficacy with 40% tumor cure at a dose of 0.47 μmol/kg. Although the PAA formulation did not enhance the PDT efficacy at similar treatment parameters, it did show a markedly improved tumor-specificity (determined by fluorescence imaging).[28] Our objective was to prepare a single platform for imaging and therapy, therefore we investigated a synthetic approach in which the PS **1** was conjugated with **3**. The resulting product showed excellent tumor-imaging ability (dose: 0.3 μmol/kg), but the therapeutic dose was eight-to tenfold higher. The low activity of the conjugate could be due

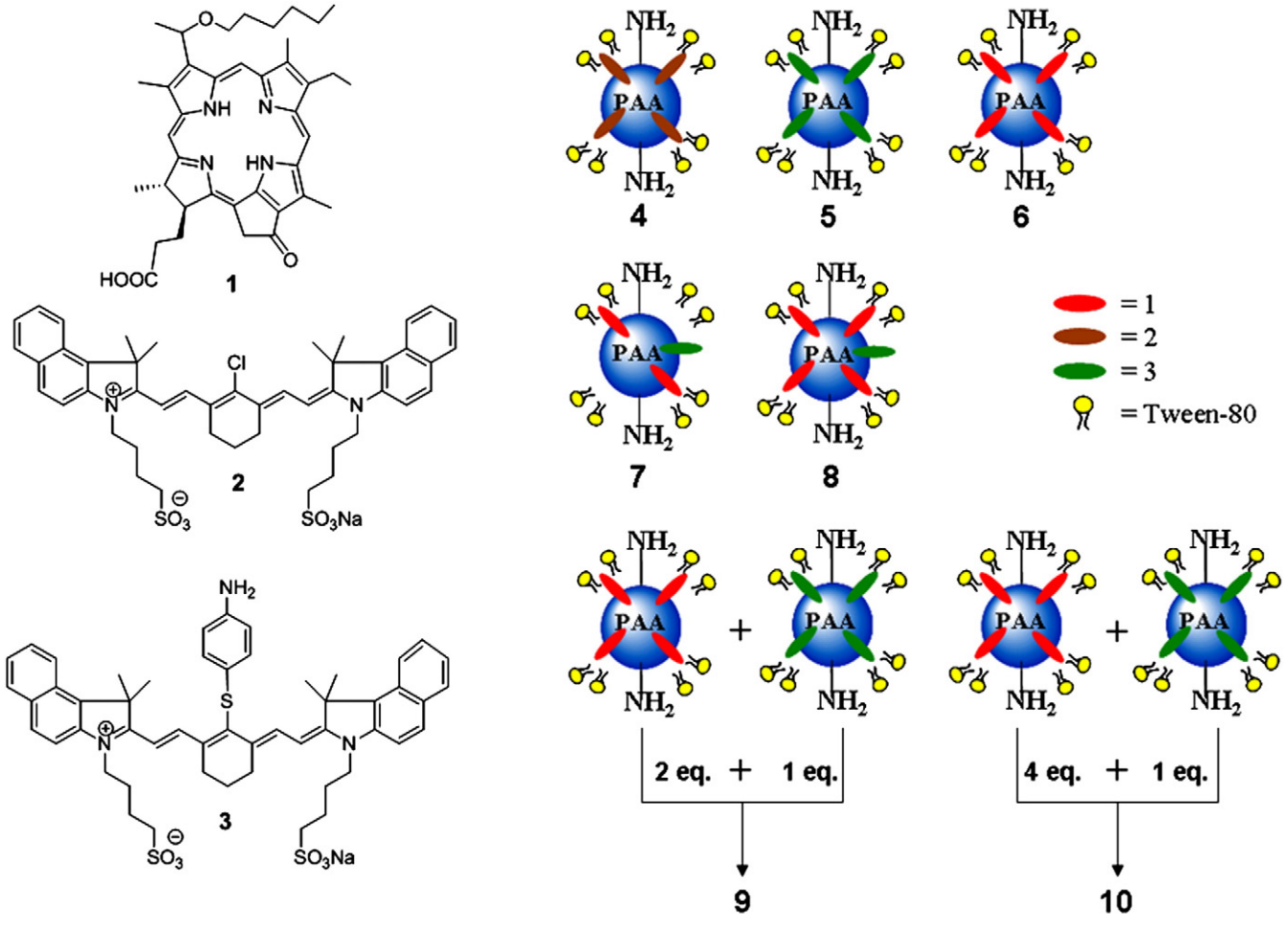

Figure 1. Post-loading of amine functionalized PAA NPs with IR-820, CD 2: nanoconstruct 4; CD 3: nanoconstruct 5; HPPH, photosensitizer 1: nanoconstruct 6; 1 and 3 at a 2:1 molar ratio: nanoconstruct 7; and 1 and 3 at a 4:1 molar ratio: nanoconstruct 8. Nanoformulation 9 and 10 is nanoconstruct 6 and 5 mixed such that the molar ratio of 1 to 3 is 2:1 and 4:1, respectively.

to a part of the singlet oxygen produced by exposing the tumors with light was quenched by the CD, which reduced its activity and thus required a higher dose of the agent (HPPH-CD) for achieving efficacy similar to PS (HPPH) **1**. HPPH-CD conjugate also exhibited significant Förster (fluorescence) resonance energy transfer (FRET), which indirectly correlates to singlet oxygen production, a key cytotoxic agent for PDT. In other words molecules with higher FRET should show reduced singlet oxygen production and PDT efficacy Figure 1.

Therefore, for our current study we were interested in preparing a series of multifunctional PAA nanoplatforms in which the PS and the CD molecules are post-loaded together in variable ratios or separately post-loaded (Figure 1, nanoconstructs **4**−**10**) and to investigate their tumor imaging and therapeutic potential. We anticipated that among all the nanoconstructs, the nanoformulation **10** in which PS and CD were separately post-loaded and then mixed in a ratio of 4 to 1 may show enhanced PDT response because of lower singlet oxygen quenching probability by the CD or the energy transfer between the two chromophores (PS and CD), which could result in higher singlet oxygen production and improved long-term tumor cure.

Characterization of PAA NPs: size, dispersion, and release kinetics

To characterize the size and dispersity of the NPs, dynamic light scattering (DLS) and scanning electron microscopy (SEM) was used. The DLS showed a mean diameter of 33.5, 32.5, and

Figure 2. Whole body fluorescence images of BALB/c mice bearing Colon-26 tumors. Control mouse **(A, E, I,** and **M)**, CD 2 **(B-D)**, nanoconstruct 4 **(F-H)**, CD 3 **(J-L)**, nanoconstruct 5 **(N-P)**, 24, 48, and 72 h post intravenous injection. The fluorescence intensity values are background subtracted from the control mouse (CD 2, **Q**, and CD 3, **R**). The error bar is the standard deviation of the mean fluorescence intensity in the tumors, $n = 3$. ∗Statistical significance of the difference in mean fluorescence intensity ($P < 0.05$, Student t test).

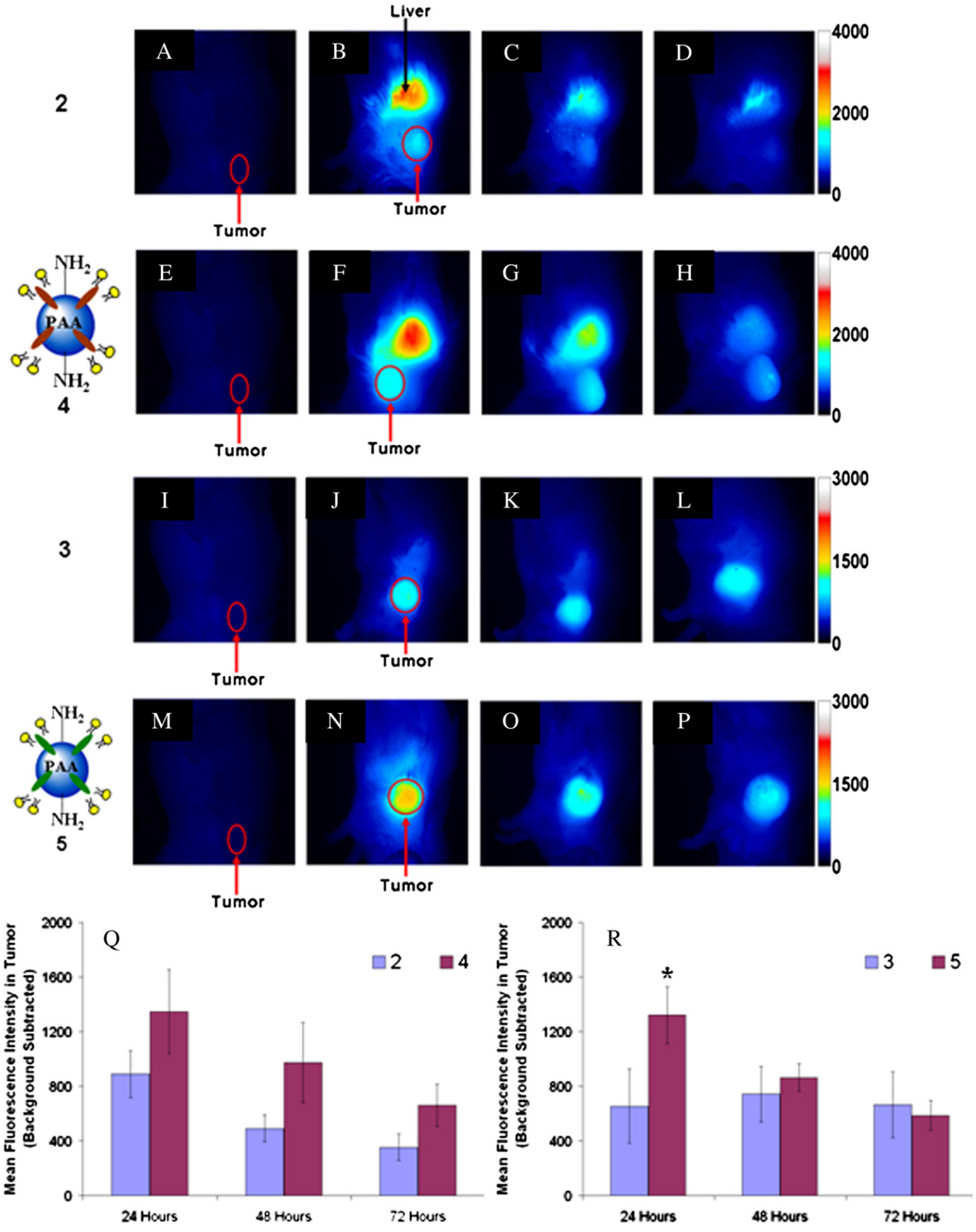
Liver
A
B
C
D
2
Tumor
Tumor
4000
2000
0
NH2
PAA
NH2
4
E
F
G
H
Tumor
Tumor
4000
2000
0
I
J
K
L
3
Tumor
Tumor
3000
1500
0
NH2
PAA
NH2
5
M
N
O
P
Tumor
Tumor
3000
1500
0
Q
Mean Fluorescence Intensity in Tumor (Background Subtracted)
2000
1600
1200
800
400
0
2
4
24 Hours
48 Hours
72 Hours
R
*
3
5
24 Hours
48 Hours
72 Hours

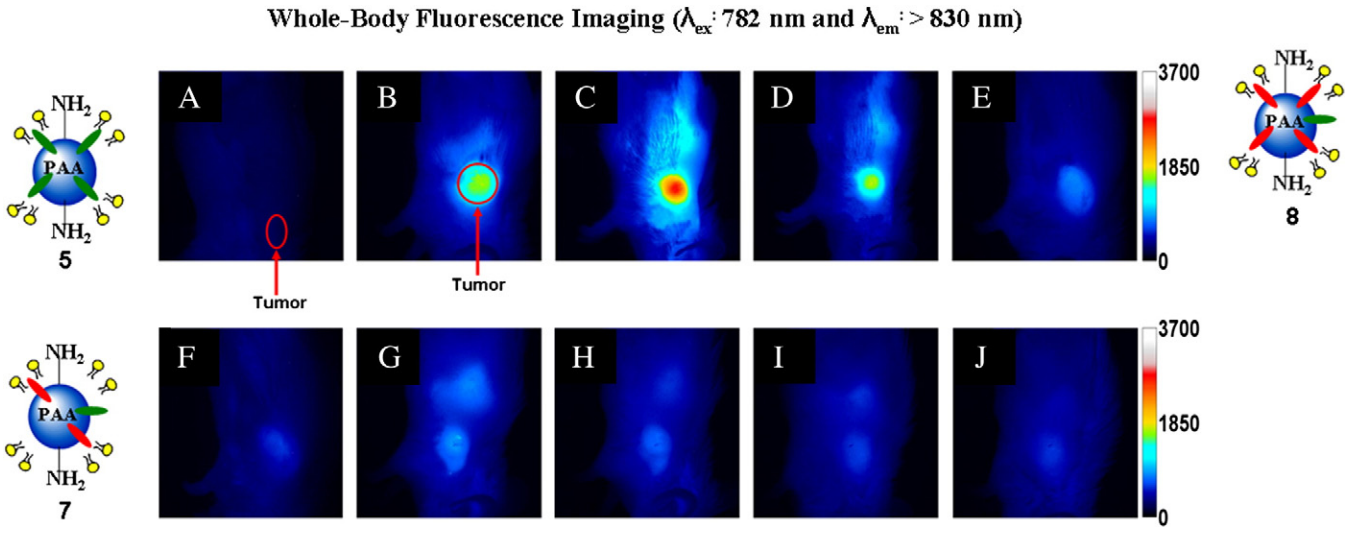

Figure 3. Whole body fluorescence images of a control mouse **(A)**, nanoconstructs/formulation 5 **(B)**, 7 **(C** and **D)**, 8 **(E** and **F)**, 9 **(G** and **H)**, and 10 **(I** and **J)** in BALB/c mice bearing Colon 26 tumors. For A-J the excitation wavelength was 782 nM. Images A, B, C, E, G, and I and D, F, H, and J were taken 24 and 48 h post-intravenous injection, respectively.

35.2 nM for blank NPs, nanoconstruct **6**, **5**, and **7**. The SEM demonstrated that the NPs are uniform and monodisperse, with a mean diameter of ~25 nM (see Supplementary Materials).

For PDT, porous NPs are advantageous since release of PS from the NP is not required for the singlet oxygen to diffuse into the tumor cells. However, if the release profile is rapid the NP may not be able to efficiently deliver a high payload of the desired agent to tumor. Therefore, we investigated the release profiles of the PS **1** and the CD **3** from nanoconstructs **5**–**10**, respectively, by incubating them in 1% HSA at variable time points. The release profiles are summarized in the Supplementary Materials. The release of PS **1** in nanoconstruct **6** showed a two-phase release, where an increase in the release was seen in the first 4 hours, which subsequently decreased during the following 20 hours. Compared with nanoconstructs **7**–**10**, nanoconstruct **6** showed the highest retention of PS **1** (HPPH) over a 24-hour period with approximately 87% being retained. When comparing the percentage of PS 1 retained (at the initial time point, time zero), on addition of 1% HSA, the nanoconstruct **8** and **10** showed the highest retention (~84%) of the PS. To mimic the release of PS **1** and CD **3** from nanoconstruct 7 in vivo, the nanoformulation **7**, which provided the best whole-body fluorescence imaging and PDT response, was also subjected for the release of both the chromophores in 25% BCS (37°C) at 4, 8, 12, and 24 hours post-addition. The maximum release (3.2%) for PS **1** occurred at the **4** hour time point, whereas for the CD **3**, the maximum release (2.8%) was observed at the 8 hour time point. These results were interesting to show a slower release of both the CD and the PS under physiologically relevant conditions.

Fluorescence imaging ability of various formulations

To show that CD **2** (IR820, Sigma-Aldrich) has poor tumor selectivity, whole body fluorescence imaging of BALB/c mice bearing subcutaneous Colon 26 tumors was performed. The water insoluble fluorophore **2** was formulated in a **1**% Tween-80/5% dextrose solution and was injected intravenously at a dose of 0.3 μmole/kg. The mice were imaged at 24, 48, and 72 hours post-injection (Figure 2, *B-D*). Because of the rather poor tumor localization of **2**, we post-loaded it into PAA NPs formulation **4** and compared their tumor uptake and fluorescence imaging abilities. The results summarized in Figure 2 clearly indicate much improved tumor selectivity of the PAA NP formulation **4** over the free fluorophore **2**. Under similar imaging parameters, modified CD **3** and the corresponding nanoconstruct **5** (CD **3** post-loaded to PAA NPs) were also imaged (Figure 2). As can be seen, compared with CD **2** (Figure 2), the modified version **3** showed higher uptake and improved tumor-imaging ability (Figure 2, *J-L*). On post-loading the CD **3** to PAA NPs, its uptake and tumor-imaging ability at 24, 48, and 72 hours post-injection was further enhanced (Figure 3, *N-P*) with the difference in intensity in the tumor for **5** being statistically higher ($P < 0.05$) at 24 hours post-injection. We then decided to investigate further the use of these biodegradable NPs in developing a "multi-functional" nanoplatform. The fluorescence imaging of PAA nanoconstructs/formulations **7**–**10** in which HPPH **1** and CD **3** were post-loaded at a ratio of 2:1 and 4:1 (either in a single NP **7** and **8** or in separate NPs **9** and **10**), respectively, was investigated in BALB/c mice bearing Colon 26 tumors. On comparing the images obtained by using the CD **3** alone and the corresponding nanoconstructs **5**, **7**–**10** the maximum accumulation in the tumor for **3** was observed at 48 hours post-injection (Figure 2, *K*), whereas the nanoconstructs produced the maximum tumor uptake at 24 hours post-injection (Figures 2 and 3). This could be due to a significant difference in the pharmacokinetic characteristics of the products in two different formulations. In nanoconstructs **7** and **8** in which the PS and CD were post-loaded in a ratio of 2 to 1 and 4 to 1 on excitation of the CD at 782 nM gave fluorescence at 866 and 870 nM, respectively. Interestingly, both nanoconstructs on in vivo excitation at 665 nM produced

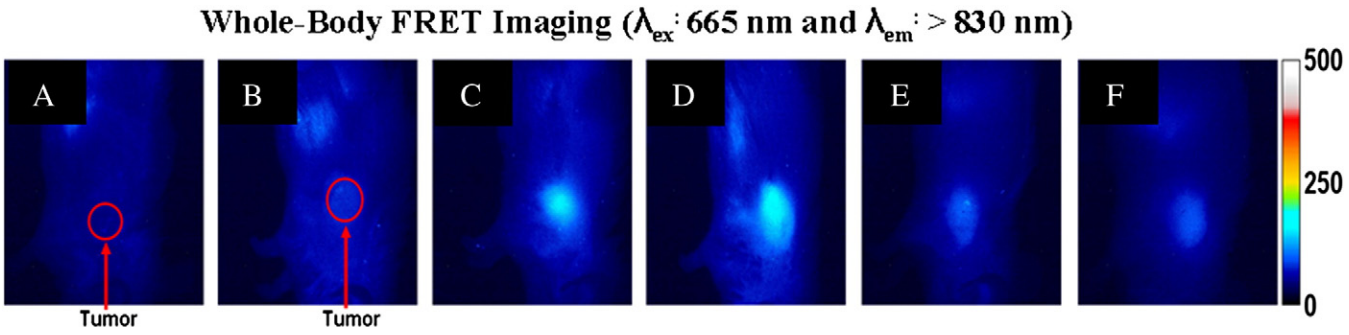

Figure 4. Whole body FRET images of a control mouse **(A)**, nanoconstructs/formulation 5 **(B)**, 7 **(C)**, 8 **(D)**, 9 **(E)**, and 10 **(F)** in BALB/c mice bearing Colon 26 tumors. For A-F the excitation wavelength was 665 nM. Images A-F were taken 24 h post-intravenous injection.

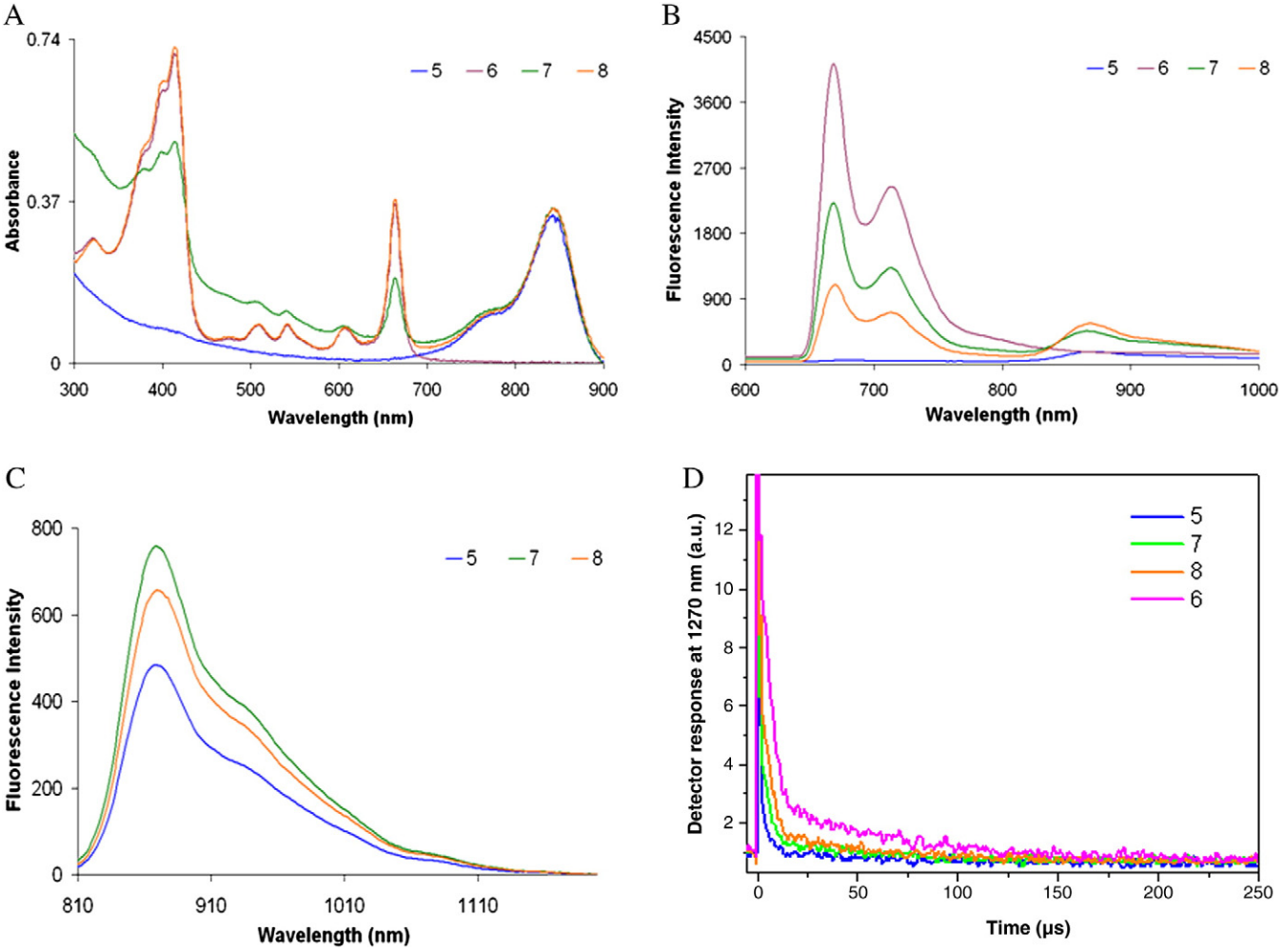

Figure 5. **(A)** Electronic absorption spectra of nanoconstructs 5, 6, 7, and 8 in water. **(B)** Fluorescence emission of nanoconstructs 5, 6, 7, and 8 excited at 532 nM in water. **(C)** Fluorescence emission of nanoconstructs 5, 7, and 8 excited at 785 nM. **(D)** The singlet oxygen production of nanoconstructs 5, 6, 7, and 8 in water was detected by measuring the phosphorescence of singlet oxygen, $^1O_2$, at 1270 nM on excitation by a 532 nM laser. Nanoconstruct 5 was used as the instrument response function (IRF) as it does not produce $^1O_2$.

a significant fluorescence beyond 860 nM, which can be explained by the phenomenon known as the FRET, or by the more general phenomena of energy migration, or excitation percolation, followed by energy trapping,[29,30] analogous to the energy transport and funneling process in photosynthetic antenna. On the basis of imaging results summarized in Figure 4, the nanoconstruct **7** provided the greatest contrast between the tumor and non-tumor tissues.

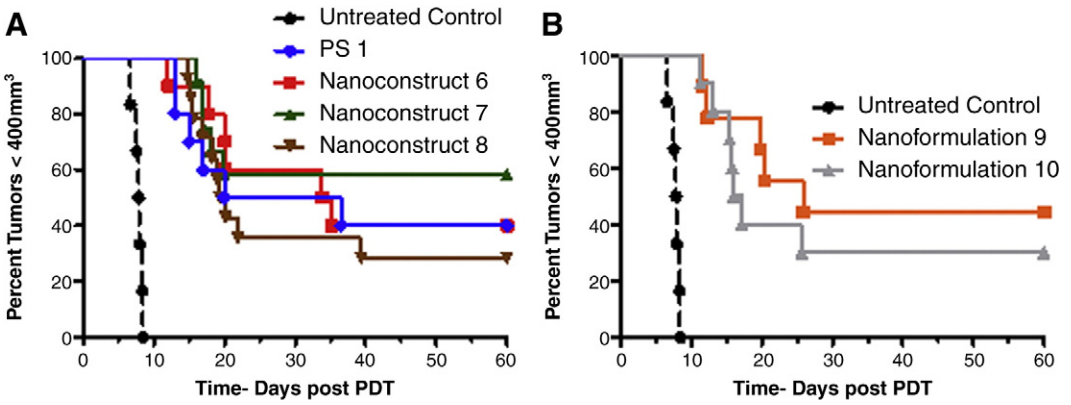

Figure 6. Kaplan-Meier plots for BALB/c mice bearing subcutaneous Colon 26 tumors treated with PS 1 and various nanoconstructs at the PS dose of 0.47 μmol/kg. The tumors were exposed to light at the light fluence and fluence rate of 135 J/cm^2 at 75 mW/cm^2. Under same treatment parameters nanoconstruct 7 (containing HPPH and CD in a ratio of 2:1) showed the best long-term PDT efficacy (six/ten mice were tumor-free on day 60).

Correlation between energy transfer and singlet oxygen production efficiency

It is known that when a PS is in close proximity to a longer wavelength-absorbing fluorophore, with a spectral overlap between the fluorescence of the PS and the absorbance of the fluorophore, then on exciting the PS, the PS fluorescence decreases because of the energy transfer to the fluorophore and the singlet oxygen yield also diminishes.[22,24] This phenomenon was evident for the nanoconstructs containing both the PS and the CD. To determine the degree of energy transfer between PS and fluorophore, the fluorescence of nanoconstructs **7** and **8** were compared with **5** and **6**. The concentration for the CD was kept constant in all nanoconstructs and the concentration of **1** for nanoconstruct **6** and **8** was kept the same and was two times higher than for nanoconstruct **7**. The fluorescence spectrum in Figure 5, *B* shows the difference in fluorescence intensity for **6**, **7**, and **8**, which resulted from the different efficiency of the PS→CD energy transfer in these nanoconstructs. This energy transfer caused a decrease in intensity of the PS fluorescence along with an increase in CD fluorescence intensity. The energy transfer was strongest for nanoconstruct **8** because the fluorescence spectrum displayed the least intense fluorescence band from PS moiety ($\lambda_{max} \approx 670$ nM) and the most intense fluorescence band from the CD moiety ($\lambda_{max} \approx 870$ nM) on excitation at 532 nM (Figure 5, *B*). Also, on excitation of **3** at 785 nM, CD fluorescence was more intense for nanoconstructs **7** and **8** than for pure CD nanoconstruct **5**, even if difference in absorption at 785 nM was minimal (Figure 5, *C*). This was an effect of the post-loaded PS molecules; their presence in the post-loaded PAA NPs could result in a more dense environment for the CD molecules, which, in turn, enhanced the radiative rate for the CD fluorophore. Overall, combination of the facts that the PS fluorescence under 532 nM excitation for **7** and **8** was less intense than for **6** and, at the same time, CD fluorescence under 532 nM excitation was more intense for **7** and **8** than for **5** unambiguously demonstrates that energy transfer PS→CD occurs in nanoconstructs and its efficiency for **8** was higher than that for **7**. This higher ET efficiency can be explained by the higher concentration of PS post-loaded to NPs resulting in less average distance between PS chromophores, allowing electronic excitation to migrate from one PS molecule to others, before being trapped by the CD chromophore. Lovell et al[31] had reported a similar observation in a series of pyropheophorbide-*a* conjugated with quenchers. An increase in concentration of the PS possibly results in a higher probability of electronic excitation energy percolation causing the trapping of the electronic excitations by lower concentration of the quenchers (CDs).

To confirm that the more efficient PS→CD energy transfer in the nanoconstructs correlates with a less efficient production of singlet oxygen, we compared the singlet oxygen generation yield of the nanoconstructs using the singlet oxygen phosphorescence spectroscopy. Phosphorescence decays are shown in Figure 5, *D* and demonstrate two clearly distinguishable decay rates for the singlet oxygen. One is shorter with a lifetime of ~4 μs (which is close to the lifetime of singlet oxygen in water[32]) suggesting that it is derived from the excited oxygen molecules decaying in aqueous environment. The second decay rate is much longer with a lifetime of ~100 μs, which is apparently associated with singlet oxygen decaying within the PAA matrix. The production of singlet oxygen was highest for the PS only formulation (nanoconstruct **6**) and decreases for three others in the order of **8**>**7**>**5**. We assume that the production of singlet oxygen by **5** was negligible because it does not contain PS; thus the decay curve for **5** practically depicts the Instrument Response Function of the setup. These results were understandable because there was twice the amount of PS in nanoconstruct **8**, which should produce more singlet oxygen, even if energy transfer from PS is more efficient in **8** than in **7**. Overall, it is important to stress that both **8** and **7** nanoconstructs showed singlet oxygen production comparable with that from the PS NP formulation, nanoconstruct **6**. These and our current results demonstrate that in a two-chromophore system, an increase in FRET and/or energy percolation increases the fluorescence intensity of the acceptor or longer wavelength (lower energy) chromophore, which decreases singlet oxygen production.[22,24]

Comparative in vivo PDT efficacy of PAA NPs containing HPPH and CD in variable ratios (nanoconstructs 6−10 versus PS 1)

HPPH, derived from chlorophyll-a, is an effective PDT agent with low skin phototoxicity and, in BALB/c mice bearing Colon 26 tumors, a complete PDT response of 40% was observed at a dose of 0.47 μmoles/kg on exposing the tumors with light at 665 nM, delivered at a fluence, and fluence-rate of 135 J/cm^2 and 75 mW/cm^2 24 hours post-injection. To compare the newly developed nanoconstructs with free HPPH, we used similar treatment parameters as described above. In preliminary screening, the PDT response (no tumor regrowth) for HPPH **1**, nanoconstructs **6**, **7**, **8**, **9**, and **10** was 40%, 40%, 60%, 30%, 40%, and 30%, respectively. The nanoconstruct **7** containing HPPH and CD **3** in a ratio of 2:1 was more effective than PS **1** alone in 1% Tween 80 formulation and nanoformulations **9** and **10**, and also provided (1) the ability to both image and treat the tumors, which could be extremely useful for a "See and Treat" approach and (2) compared with the synthetic HPPH-CD conjugate in which the imaging dose was eight-to tenfold lower than the therapeutic dose, a single dose (0.47 μmoles/kg) of nanoconstruct **7** can be used for both tumor imaging and PDT Figure 6.

Discussion

In our hands, compared with encapsulation,[29] the post-loading approach was more effective when hydrophobic compounds were used in conjunction with PAA NPs. PAA NPs provide a great platform for post-loading because of the porous nature of the polyacrylamide-based hydrogels, wherein the hydrophobic part of the molecule may interact preferentially. We have found that the surfactant Tween-80 plays an important role in efficient retention of the compounds within the NPs. Its presence in an aqueous solution apparently causes formation of a micellar layer on the nanoconstruct surface, whereby the polyethers form the outer hydrophobic layer and the oleic acid forms the inner, more hydrophobic layer of the construct.

Among all organic NIR fluorophores, CDs in general have shown great potential for fluorescence imaging.[30] In this series of compounds, IR820, a NIR CD, is of particular interest because of its inherent desirable photophysical characteristics, namely, excitation and emission in the NIR range beyond 750 nM, which allows for deeper tissue penetration of activating light; however, its tumor uptake is known to be low.

Burns et al,[28] have shown that when Cy5 was encapsulated within PEG-coated silica NPs (3.3 and 6.0 nM diameter, respectively), the fluorescence intensity of the dye increased by 2.0–2.5 times, compared with that of the free dye. This prompted us to investigate the use of PAA nanoconstructs for the delivery of both imaging and therapeutic agents. We found that the newly constructed NPs were capable of delivering a high payload of both the PS and CD molecules to the tumor. This is likely due to the EPR effect.[33,34]

The UV-Visible and fluorescence spectrometry studies confirmed that both hydrophobic PS and hydrophilic fluorophores related to CDs can be co-loaded into amine functionalized PAA nanoconstructs and maintain their photophysical characteristics. The DLS and SEM images show that on co-post-loading, the diameter and spherical shape of the NPs remain intact. The in vitro spectroscopic measurements show that excitation of nanoconstruct **8** channels more energy transport/-FRET from HPPH to CD, resulting in reduced efficiency of **1** for PDT efficacy. In contrast to synthetic HPPH-CD conjugates, a single dose of the PAA nanoconstruct can be used simultaneously for tumor imaging and for efficient long-term tumor cure by PDT. In addition, nanoconstructs **9** and **10** produced lower in vivo FRET signal as compared with nanoconstructs **7** and **8**; however, the nanoconstruct **7** still provided the best PDT outcome (60% for PS 1 versus 40% for nanoconstruct **6**). Further studies to improve the target-specificity of the nanoconstructs by introducing certain target-specific agents at the periphery of the PAA NPs are in progress.[35]

Acknowledgments

The authors thank Dr. Arindam Sen, RPCI, for helpful discussions and allowing us to use his research facility for determining the size of the nanoparticles.

Appendix A. Supplementary data

Supplementary data associated with this article can be found, in the online version, at doi:10.1016/j.nano.2011.11.011.

References

1. Brown SB, Brown EA, Walker I. The present and future role of photodynamic therapy in cancer treatment. Lancet Oncol 2004;5: 497-508.
2. Chen B, Pogue BW, Luna JM, Hardman RL, Hoopes PJ, Hasan T. Tumor vascular permeabilization by vascular-targeting photosensitization: effects, mechanism, and therapeutic implications. Clin Cancer Res 2006;12:917-23.
3. Dougherty TJ, Gomer CJ, Henderson BW, Jori G, Kessel D, Korbelik M, et al. Photodynamic therapy. J Natl Cancer Inst 1998;90:889-905.
4. Dolmans DE, Fukumura D, Jain RK. Photodynamic therapy for cancer. Nat Rev Cancer 2003;3:380-7.
5. Biel M. Advances in photodynamic therapy for the treatment of head and neck cancers. Lasers Surg Med 2006;38:349-55.
6. Henderson BW, Gollnick SO. Mechanistic principles of photodynamic therapy. In: Vo-Dinh T, editor. Biomedical photonics handbook. Boca Raton: CRC Press; 2002.
7. Korbelik M, Sun J. Cancer treatment by photodynamic therapy combined with adoptive immunotherapy using genetically altered natural killer cell line. Int J Cancer 2001;93:269-74.
8. Pandey RK, Goswami LN, Chen Y, Gryshuk A, Missert JR, Oseroff A, et al. Nature: a rich source for developing multifunctional agents: tumor-imaging and photodynamic therapy. Lasers Surg Med 2006;38:445-67.
9. Pandey RK, James NS, Chen Y, Missert J, Sajjad M. Bifunctional agents for imaging and therapy. In: Gomer C, editor. Methods in molecular biology. Vol 635, photodynamic therapy, methods and protocols. New York: Springer; 2010.
10. Hamlin MR. In: Hamblin MR, Mroz P, editors. Covalent photosensitizer conjugates, part 1: antibodies and other protein for targeted photodynamic therapy in Advances in Photodynamic Therapy. Boston: Artech House; 2008.
11. Kopelman R, Philbert M, Koo YEL, Moffat BA, Reddy GR, McConville P, et al. Multifunctional nanoparticle platforms for in vivo MRI

enhancement and photodynamic therapy of a rat brain cancer. J Magn Magn Mater 2005;293:404-10.
12. Weissleder R. A clearer vision for in vivo imaging. Nat Biotechnol 2001;19:316-7.
13. Frangioni JV. In vivo near-infrared fluorescence imaging. Curr Opin Chem Biol 2003;7:626-34.
14. Pandey RK, Sumlin AB, Potter WR, Bellnier DA, Henderson BW, Constantine S, et al. Structure and photodynamic efficacy among alkyl ether analogues of chlorophyll-a derivatives. Photochem Photobiol 1996;63:194-205.
15. Henderson BW, Bellnier DA, Greco WR, Sharma A, Pandey RK, Vaughan L, et al. An in vivo quantitative structure-activity relationship for a congeneric series of pyropheophorbide derivatives as photosensitizers for photodynamic therapy. Cancer Res 1997;57:4000-7.
16. Bellnier DA, Henderson BW, Pandey RK, Potter WR, Dougherty TJ. Murine pharmacokinetics and antitumor efficacy of the photodynamic sensitizer 2-[1-hexyloxyethyl]-2-devinyl pyropheophorbide-a. J Photochem Photobiol 1993;20:55-61.
17. Loewen GM, Pandey RK, Bellnier D, Henderson BW, Dougherty TJ. Endobronchial photodynamic therapy for lung cancer. Laser Surg Med 2006;38:364-70.
18. Bellnier DA, Greco WR, Nava H, Loewen GM, Oseroff AR, Dougherty TJ. Mild skin photosensitivity in cancer patients following injection of Photochlor (2-[1-hexyloxy ethyl]-2-devinyl pyropheophorbide-a; HPPH) for photodynamic therapy. Cancer Chemother Pharmacol 2004;57:40-5.
19. Bellnier DA, Greco WR, Loewen GM, Oseroff AO, Pandey RK, Dougherty TJ. Population pharmacokinetics of the photodynamic therapy agent 2-[1-hexyloxyethyl]-2 devinyl pyropheophorbide-a in cancer patients. Cancer Res 2003;63:1806-13.
20. Chen Y, Gryshuk A, Achilefu S, Ohulchanskyy T, Potter W, Zhong T, et al. A novel approach to a bifunctional photosensitizer for tumor Imaging and phototherapy. Bioconjugate Chem 2005;16:1264-74.
21. Chen Y, Ohkubo K, Zhang M, Liu W, Pandey SK, Ciesielski M, et al. Photophysical, electrochemical characteristics and cross-linking of STAT-3 protein by an efficient bifunctional agent for fluorescence image-guided photodynamic therapy. Photochem Photobiol Sci 2007;6:1257-67.
22. Wenger Y, Schneider RJ, Reddy GR, Kopelman R, Jolliet O, Philbert MA. Tissue distribution and pharmacokinetics of stable polyacrylamide nanoparticles following intravenous injection in the rat. Toxicol Appl Pharmacol 2011;251:181-90.
23. Gao D, Xu H, Philbert MA, Kopelman R. Bioeliminable nanohydrogels for drug delivery. Nano Lett 2008;8:3320-4.
24. Meng H, Xue M, Xia T, Ji Z, Tarn DY, Zink JI, et al. Use of size and a copolymer design feature to improve the biodistribution and the enhanced permeability and retention effect of doxorubicin-loaded mesoporous silica nanoparticles in a murine xenograft tumor model. ACS Nano 2011;5:4131-44.
25. Matsumura Y, Maeda H. A new concept for macromolecular therapeutics in cancer chemotherapy: mechanism of tumoritropic accumulation of proteins and the antitumor agent smancs. Cancer Res 1986;46:6387-92.
26. Nasongkla N, Bey E, Ren J, Ai H, Khemtong C, Guthi JS, et al. Multifunctional polymeric micelles as cancer-targeted, MRI-ultrasensitive drug delivery systems. Nano Lett 2006;6:2427-30.
27. Wang S, Fan W, Kim G, Hah HJ, Lee YEK Kopelman R, et al. Novel methods to incorporate photosensitizers into nanocarriers for cancer treatment by photodynamic therapy. Lasers Surg Med 2011; 43:686-95.
28. Burns AA, Vider J, Ow H, Herz E, Penate-Medina O, Baumgart M, et al. Fluorescent silica nanoparticles with efficient urinary excretion for nanomedicine. Nano Lett 2009;9:442-8.
29. Kopelman R. Exciton percolation in mixed molecular crystals and aggregates: from naphthalene to photosynthesis. J Phys Chem 1976;80:2191-5.
30. Hoshen J, Kopelman R. Exciton percolation I: migration dynamics. J Chem Phys 1976;65:2817-23.
31. Lovell JF, Chen J, Jarvi MT, Cao WG, Allen AD, Liu Y, et al. FRET quenching of photosensitizer singlet oxygen generation. J Phys Chem B 2009;113:3203-11.
32. Ohulchanskyy T, Roy I, Goswami LN, Bergey EJ, Pandey RK, Oseroff AR, et al. Organically modified silica nanoparticles with covalently incorporated photosensitizer for photodynamic therapy of cancer. Nano Lett 2007;7:2835-42.
33. Thurber GM, Figruiredo JL, Weissleder R. Detection limits of intraoperative near infrared imaging for tumor resection. J Surg Oncol 2010;102:758-64.
34. Rao J, Dragulescu-Andrasi A, Yao H. Fluorescence imaging in vivo: recent advances. Curr Opin Biotechnol 2007;18:17-25.
35. Wisner I, Wang S, Lee YEK, Fan W, Gong Y, Burgos-Ojeda D, et al. F3-targeted cisplatin-hydrogel nanoparticles as an effective therapeutic that targets both murine and human ovarian tumor endothelial cells in vivo. Cancer Res 2010;70:8674-83.